



Article

# Biochemical Characterization and Complete Conversion of Coenzyme Specificity of Isocitrate Dehydrogenase from *Bifidobacterium longum*

Shi-Ping Huang <sup>†</sup>, Hong-Mei Cheng <sup>†</sup>, Peng Wang and Guo-Ping Zhu <sup>\*</sup>

The Research Center of Life Omics and Health and Anhui Provincial Key Laboratory of the Conservation and Exploitation of Biological Resources, Anhui Normal University, Wuhu 241000, Anhui, China;

huangsp2014@gmail.com (S.-P.H.); chengmei325111@163.com (H.-M.C.); wangpeng1219@yahoo.com (P.W.)

<sup>\*</sup> Correspondence: gpz1996@yahoo.com; Tel.: +86-553-388-3539; Fax: +86-553-388-3592

<sup>†</sup> These authors contributed equally to this work.

Academic Editor: Ritva Tikkanen

Received: 10 January 2016; Accepted: 19 February 2016; Published: 26 February 2016

**Abstract:** *Bifidobacterium longum* is a very important gram-positive non-pathogenic bacterium in the human gastrointestinal tract for keeping the digestive and immune system healthy. Isocitrate dehydrogenase (IDH) from *B. longum* (*BlIDH*), a novel member in Type II subfamily, was overexpressed, purified and biochemically characterized in detail. The active form of *BlIDH* was an 83-kDa homodimer. Kinetic analysis showed *BlIDH* was a NADP<sup>+</sup>-dependent IDH (NADP-IDH), with a 567- and 193-fold preference for NADP<sup>+</sup> over NAD<sup>+</sup> in the presence of Mg<sup>2+</sup> and Mn<sup>2+</sup>, respectively. The maximal activity for *BlIDH* occurred at 60 °C (with Mn<sup>2+</sup>) and 65 °C (with Mg<sup>2+</sup>), and pH 7.5 (with Mn<sup>2+</sup>) and pH 8.0 (with Mg<sup>2+</sup>). Heat-inactivation profiles revealed that *BlIDH* retained 50% of maximal activity after incubation at 45 °C for 20 min with either Mn<sup>2+</sup> or Mg<sup>2+</sup>. Furthermore, the coenzyme specificity of *BlIDH* can be completely reversed from NADP<sup>+</sup> to NAD<sup>+</sup> by a factor of 2387 by replacing six residues. This current work, the first report on the coenzyme specificity conversion of Type II NADP-IDHs, would provide better insight into the evolution of NADP<sup>+</sup> use by the IDH family.

**Keywords:** *Bifidobacterium longum*; isocitrate dehydrogenase; biochemical characterization; coenzyme specificity determinants; kinetics

## 1. Introduction

Isocitrate dehydrogenase (IDH) belongs to an ancient and ubiquitous metal-dependent  $\beta$ -decarboxylating dehydrogenase family that plays critical roles in amino acid biosynthesis, vitamin production and energy metabolism [1–3]. IDHs are key enzymes in the tricarboxylic acid cycle (TCA cycle) that catalyze the oxidative decarboxylation of isocitrate to  $\alpha$ -ketoglutarate ( $\alpha$ -KG) and CO<sub>2</sub> with NAD<sup>+</sup> or NADP<sup>+</sup> as a coenzyme [4]. According to the different coenzyme dependencies, IDHs play a variety of roles *in vivo*. NAD<sup>+</sup>-dependent IDH (NAD-IDH, EC 1.1.1.41) provides the first connection between TCA cycle and electron-transport pathway by producing NADH, which participates in energy metabolism [5]. NADP<sup>+</sup>-dependent IDH (NADP-IDH, EC 1.1.1.42) generates NADPH, which provides the reducing power for biosynthesis, maintains the redox state of the cell, and takes part in CO<sub>2</sub> assimilation. Therefore, NADP-IDH is essential in glutathione metabolism, fatty acids and steroids biosynthesis, and cellular antioxidation systems [6–8]. Recently, increasing attention has been paid to human NADP-IDHs. It has been reported that the mutations at some active sites can confer a new function on NADP-IDHs to reduce  $\alpha$ -ketoglutarate to 2-hydroxyglutarate, which correlates closely with the incidence of tumors [9–11], such as gliomas, the most common type of human brain cancers.

Based on the phylogenetic analysis, IDHs can be divided into three subfamilies: Type I IDHs, Type II IDHs and monomeric IDHs [12]. Most bacterial homodimeric NAD(P)-IDHs, homotetrameric NAD-IDHs and mitochondrial heterologomeric NAD-IDHs are clustered into the Type I subfamily. The homodimeric NADP-IDHs from eukaryotes (in cytoplasm and mitochondria) and some bacterial NADP-IDHs are categorized into the Type II subfamily. It was noted that, recently, several algae IDHs were found to be Type II NAD-IDHs, whose coenzyme specificity can be completely converted from NAD<sup>+</sup> to NADP<sup>+</sup> by rational mutagenesis [12,13]. All monomeric enzymes, either NAD<sup>+</sup> or NADP<sup>+</sup>-dependent, fall into the third subfamily. Type II NADP-IDHs from eukaryotes, such as yeast, pig and human have been extensively studied, including biochemical properties, the crystal structures and catalytic mechanisms [14–16]. On the contrary, the information of Type II NADP-IDHs from bacteria is very limited and only a few of them have been preliminarily characterized.

Furthermore, it was proposed that NAD<sup>+</sup> use is an ancestral trait and NADP<sup>+</sup> use by bacterial IDHs arose on or about the time that eukaryotic mitochondria first appeared, some 3.5 billion years ago [17]. The switch in coenzyme dependency from NAD<sup>+</sup> to NADP<sup>+</sup> by IDHs was an ancient adaptation for bacterial survival on energy-poor compound (such as acetate). This hypothesis has been proved by the competition experiment in the laboratory for NADP<sup>+</sup>-dependent IDH from *Escherichia coli* (*EcIDH*), a typical member of Type I IDHs subfamily [17]. It is an interesting question that whether the selective mechanism of this ancient adaptation is also suitable to Type II IDHs subfamily, because the sequence similarity between two IDHs subfamilies is very low (<20%).

*Bifidobacterium longum*, a gram-positive and non-pathogenic bacterium, is one of the most popular probiotics in various dairy products to provide enormous health benefits for the healthy human gastrointestinal system, such as improving lactose tolerance, preventing diarrhea and inhibiting pathogen colonization [18–21]. Several studies have shown that *B. longum* plays a key role in modulating the immune system [22,23] and has certain guiding significance to cancer gene therapy [24,25].

In this work, the enzymology of a homodimeric IDH from *B. longum* (*BlIDH*) in Type II subfamily was investigated in detail. In addition, the coenzyme specificity of *BlIDH* was converted from NADP<sup>+</sup> to NAD<sup>+</sup> by site-directed mutagenesis, which may provide useful clues to explore the acquired cause of NADP<sup>+</sup> dependency by Type II IDHs.

## 2. Results

### 2.1. Sequence Alignment

The coding sequence of *BlIDH* consisted of 1221 bp nucleotides with one open reading frame (ORF) encoding a protein of 406 amino acids. This enzyme showed a high level of sequence similarity to that of Type II NADP-IDHs, such as *Mycobacterium tuberculosis* IDH (73.5%), *Clostridium thermocellum* IDH (53.8%) and human cytosolic IDH (61.5%). Phylogenetic analysis was performed to further clarify the evolutionary relationship between *BlIDH* and other IDHs. The result revealed that *BlIDH* was clustered into the clade of Type II NADP-IDHs (Figure 1).

In order to evaluate potential substrate and coenzyme-binding sites, multiple sequence alignments were performed (Figure 2). All amino acids involved in substrate binding are highly conserved in both Type I and II subfamilies, but the residues responsible for coenzyme binding are significantly different in the two subfamilies. When compared with NADP-IDH in the Type II subfamily, Arg314 and His315 in the binary complex of human cytosolic NADP-IDH (*HcIDH*) are considered to be the major determinants of coenzyme specificity, which form salt bridges with the 2'-phosphate group of NADP<sup>+</sup> [15].

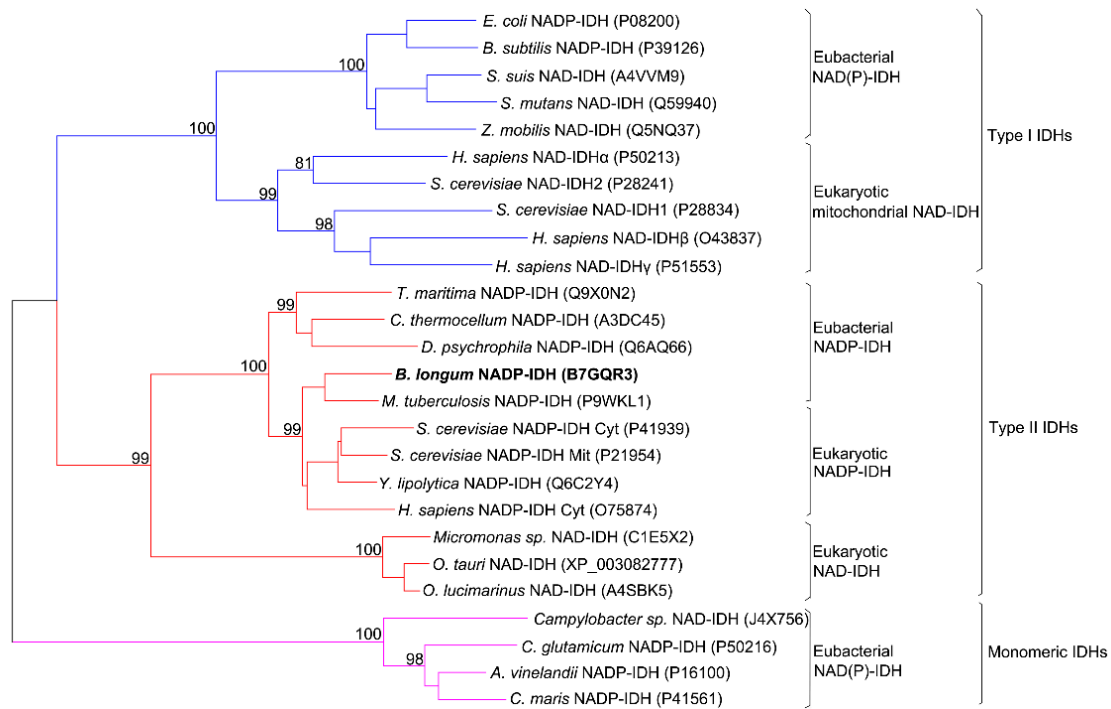


**Figure 1.** Phylogenetic tree of 26 isocitrate dehydrogenases (IDHs). A neighbor-joining tree with 500 bootstrap was created using MEGA 6.06. The GenBank accession numbers were noted in the parentheses.

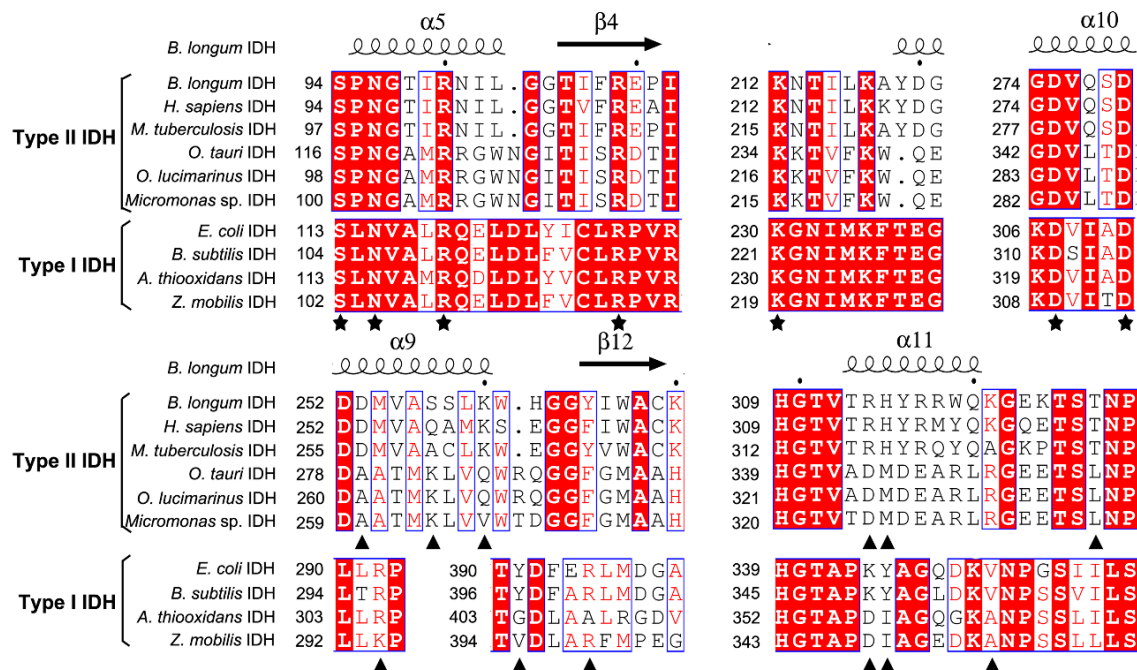


**Figure 2.** Structure-based protein sequences alignment of isocitrate dehydrogenase (IDH) from *B. longum* (BIIDH) with other IDHs. The primary residues involved in substrate binding are indicated by pentagrams (★). The residues interact with the 2'-phosphate of NADP<sup>+</sup> directly or indirectly are indicated by triangles (▲). The letters in blue boxes indicate conserved residues, and the white letters with red background in blue boxes indicate strictly conserved residues. The black letters in white boxes indicate similarity. The structure of BIIDH was generated by SWISS-MODEL server. The figure created by ESPript 3.0.

The corresponding residues are completely conserved in *BIIIDH* (Arg314 and His315). In the quaternary complex of *HcIDH* (Figure 3), the side chains of Gln257' and Lys260' (the prime indicates the other subunit of the homodimer) form hydrogen bonds with the 2'-phosphate group of NADP<sup>+</sup>, which are homologous to Ser257' and Lys260' in *BIIIDH* [15]. Furthermore, Arg314 in *HcIDH* forms a salt bridge with Asp253' (equivalent to Asp253' in *BIIIDH*) and interacts with Arg249' and Gln257' [15]. As compared with NAD-IDH, Arg314 and His315 in *BIIIDH* are replaced by Asp357 and Ile358 in *Acidithiobacillus thiooxidans* NAD-IDH (*AtIDH*) from Type I subfamily [26] and Asp344 and Met345 in *Ostreococcus tauri* NAD-IDH (*OtIDH*) from Type II subfamily [13]. Asp253', Ser257' and Lys260' in *BIIIDH* are substituted with Ala279', Lys283' and Gln286' in *OtIDH*, as shown in Figure 3.

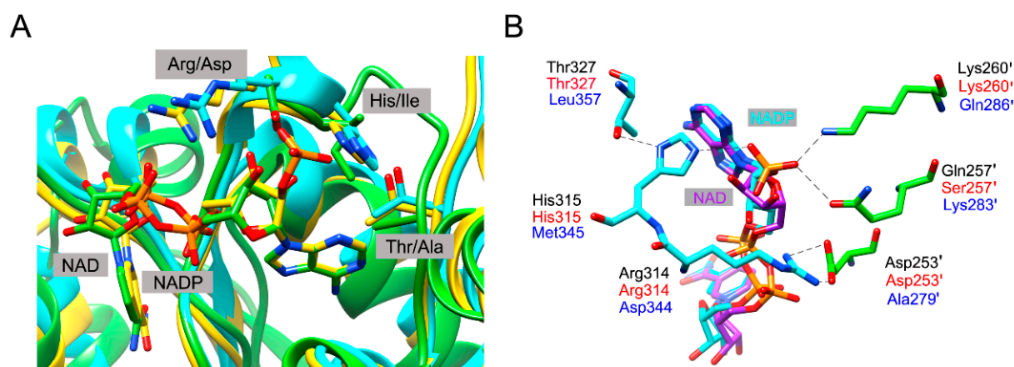


**Figure 3.** Comparison of the NADP<sup>+</sup>-binding sites among the human cytosolic NADP-IDH (*HcIDH*), *BIIIDH*, *Acidithiobacillus thiooxidans* NAD-IDH (*AtIDH*) and *Ostreococcus tauri* NAD-IDH (*OtIDH*). (A) Overlay of the subunits of *HcIDH* (yellow, PDB code: 1T0L), modelled *BIIIDH* (cyan) and *AtIDH* (green, PDB code: 2D4V) highlighting the selected coenzyme binding sites in these three IDHs. The NADP<sup>+</sup> molecule (with yellow C atoms) and NAD<sup>+</sup> molecule (with green C atoms) were represented by the stick. The model of *BIIIDH* was generated by SWISS-MODEL server; (B) A close-up view showing the selected residues involving in NADP<sup>+</sup> binding in *HcIDH* (labelled by black). The equivalent residues in *BIIIDH*, targeted by site-directed mutagenesis, and in *OtIDH* were labelled by red and blue, respectively.

## 2.2. Expression and Purification

Recombinant *BIIIDH* with 6×His tag was successfully heterologously expressed in *E. coli* Rosetta (DE3) and purified to homogeneity by Co<sup>2+</sup> affinity chromatography. Molecular mass of the recombinant protein was determined to be approximately 45 kDa by SDS-PAGE, which compared well with the predicted value (45 kDa) (Figure 4A) and was confirmed by Western blotting by probing with anti-6×His antibody (Figure 4B). The oligomeric status of *BIIIDH* was determined by size exclusion chromatography (SEC), and a single symmetrical peak was observed (Figure 4C) while the native molecular mass of *BIIIDH* was calculated to be 83 kDa, suggesting that the native enzyme forms a homodimer in solution.

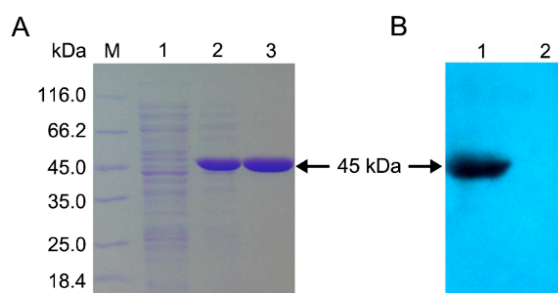


**Figure 4.** Cont.

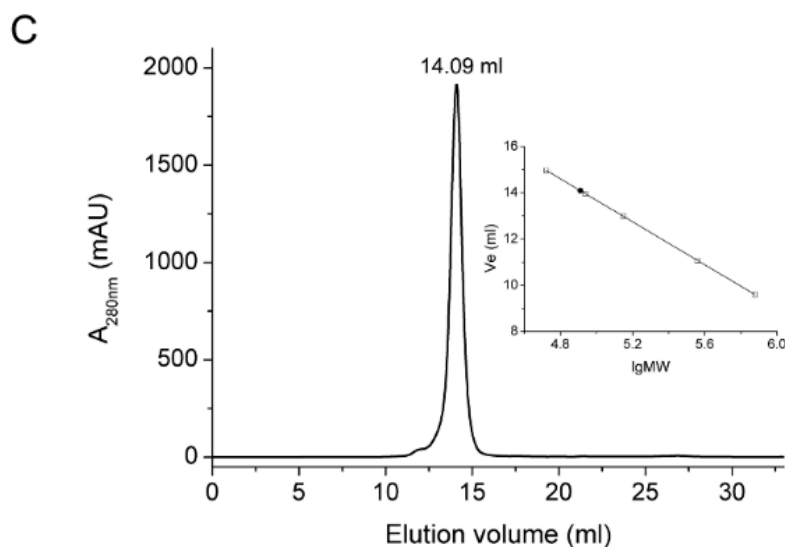


**Figure 4.** Overexpression and molecular mass determination of *BIIIDH*. (A) SDS-PAGE analysis. M, molecular mass marker; lane 1, crude extract from cells transformed by pET-28b(+) with IPTG treatment; lane 2, crude extract from cells transformed by recombinant plasmid pET-*BIIIDH* with IPTG treatment; lane 3, purified *BIIIDH*; (B) Western blot analysis. Lane 1, purified *BIIIDH*; lane 2, negative control, crude extract from cells transformed by pET-28b(+) with IPTG treatment; (C) Size exclusion chromatography (SEC) analysis of *BIIIDH*.

### 2.3. Kinetic Characterization

The optimal pH values of the purified recombinant *BIIIDH* were 7.5 with  $Mn^{2+}$  and 8.0 with  $Mg^{2+}$  (Figure 5A), similar to the homodimeric NADP-IDH from *Leptospira interrogans* (pH 7.0 with  $Mn^{2+}$  and pH 8.0 with  $Mg^{2+}$ ) [27], but apparently lower than the monomeric IDHs from *Corynebacterium glutamicum* (pH 9.0 with  $Mg^{2+}$ ) [28] and *Chlorobium limicola* (pH 9.0 with  $Mg^{2+}$ ) [29].

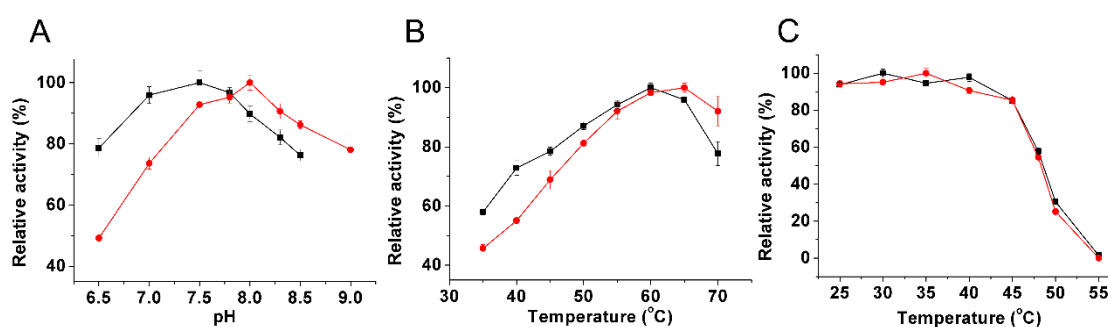


**Figure 5.** Effect of pH and temperature on the activity of *BIIIDH* in the presence of  $Mg^{2+}$  (●) and  $Mn^{2+}$  (■), respectively. (A) Effect of pH on the activity of *BIIIDH*; (B) Effect of temperature on the activity of *BIIIDH*; (C) Heat-inactivation profiles of the *BIIIDH*. The values indicate the means of at least three independent measurements.

The recombinant *BIIIDH* exhibited the maximal activity around 60 and 65 °C in the presence of  $Mn^{2+}$  and  $Mg^{2+}$ , respectively (Figure 5B), similar to that of *L. interrogans* IDH (60 °C with  $Mn^{2+}$  and  $Mg^{2+}$ ) [27], but higher than those of NAD-IDHs from *Congregibacter litoralis* (35 °C with  $Mn^{2+}$  and  $Mg^{2+}$ ) [30] and *Zymomonas mobilis* IDH (55 °C with  $Mn^{2+}$  and  $Mg^{2+}$ ) [31]. Heat-inactivation studies revealed that the recombinant *BIIIDH* was stable under 45 °C, but rapidly lost activity above this temperature, and only 50% activity remained after a 20 min incubation at 48 °C (Figure 5C).

The effects of 11 metal ions on *BIIIDH* activity were also examined. The activity of recombinant *BIIIDH* was entirely dependent on the presence of a divalent cation, such as  $Mn^{2+}$ , the most effective activator for *BIIIDH* catalysis (Table 1). However, several divalent metal ions, including  $Ni^{2+}$ ,  $Co^{2+}$ ,  $Zn^{2+}$ ,  $Cu^{2+}$  and  $Ca^{2+}$ , inhibited the activity in the presence of  $Mn^{2+}$  or  $Mg^{2+}$ , where  $Zn^{2+}$  showed the most inhibitory effects on *BIIIDH* activity.

**Table 1.** Effects of metal ions on the activity of recombinant *BIIIDH*.

| Metal Ions | Relative Activity (%) | Metal Ions          | Relative Activity <sup>1</sup> (%) | Metal Ions          | Relative Activity <sup>2</sup> (%) |
|------------|-----------------------|---------------------|------------------------------------|---------------------|------------------------------------|
| $Mn^{2+}$  | 100.00 ± 1.07         | $Mn^{2+}$           | 100.00 ± 1.07                      | $Mg^{2+}$           | 100.00 ± 0.82                      |
| $Mg^{2+}$  | 69.23 ± 0.82          | $Mn^{2+} + Mg^{2+}$ | 69.17 ± 0.41                       | $Mg^{2+} + Mn^{2+}$ | 99.92 ± 0.41                       |
| $Ni^{2+}$  | 5.67 ± 0.54           | $Mn^{2+} + Ni^{2+}$ | 47.42 ± 1.08                       | $Mg^{2+} + Ni^{2+}$ | 43.37 ± 1.46                       |
| $Co^{2+}$  | 14.30 ± 0.39          | $Mn^{2+} + Co^{2+}$ | 30.80 ± 0.40                       | $Mg^{2+} + Co^{2+}$ | 39.58 ± 0.10                       |
| $Zn^{2+}$  | 0                     | $Mn^{2+} + Zn^{2+}$ | 5.19 ± 0.38                        | $Mg^{2+} + Zn^{2+}$ | 11.02 ± 0.13                       |
| $Cu^{2+}$  | 0                     | $Mn^{2+} + Cu^{2+}$ | 31.04 ± 0.37                       | $Mg^{2+} + Cu^{2+}$ | 61.38 ± 0.67                       |
| $Ca^{2+}$  | 0                     | $Mn^{2+} + Ca^{2+}$ | 62.33 ± 0.50                       | $Mg^{2+} + Ca^{2+}$ | 14.06 ± 0.50                       |
| $Li^{+}$   | 0                     | $Mn^{2+} + Li^{+}$  | 103.83 ± 0.65                      | $Mg^{2+} + Li^{+}$  | 100.52 ± 0.65                      |
| $Rb^{+}$   | 5.26 ± 0.39           | $Mn^{2+} + Rb^{+}$  | 96.09 ± 0.57                       | $Mg^{2+} + Rb^{+}$  | 105.77 ± 0.35                      |
| $K^{+}$    | 4.89 ± 0.11           | $Mn^{2+} + K^{+}$   | 101.98 ± 0.30                      | $Mg^{2+} + K^{+}$   | 103.75 ± 0.90                      |
| $Na^{+}$   | 6.05 ± 0.43           | $Mn^{2+} + Na^{+}$  | 104.53 ± 0.15                      | $Mg^{2+} + Na^{+}$  | 109.27 ± 0.18                      |

<sup>1</sup> The activity in the presence of  $Mn^{2+}$  alone is regarded as a 100% value for this column; <sup>2</sup> The activity in the presence of  $Mg^{2+}$  alone is regarded as a 100% value for this column. The values indicate the means of at least three independent measurements.

The kinetic parameters for recombinant *BIIIDH* were determined in both  $NAD^{+}$ - and  $NADP^{+}$ -dependent forms (Table S1). The  $K_m$  values of *BIIIDH* for  $NADP^{+}$  were 19.45  $\mu M$  with  $Mg^{2+}$  and 58.29  $\mu M$  with  $Mn^{2+}$  (Figure S1A,B). The apparent  $K_m$  values of *BIIIDH* for  $NAD^{+}$  were over 184-fold and nine-fold higher than those for  $NADP^{+}$  in the presence of  $Mg^{2+}$  and  $Mn^{2+}$ , respectively. As a result, the catalytic efficiency ( $k_{cat}/K_m$ ) of *BIIIDH* showed 567-fold ( $Mg^{2+}$ ) and 193-fold ( $Mn^{2+}$ ) preference for  $NADP^{+}$  over  $NAD^{+}$ , respectively. Evidently, *BIIIDH* has remarkably high coenzyme specificity toward  $NADP^{+}$  although it is a dual-specificity enzyme.

When compared with other homodimeric  $NADP$ -IDHs, the  $K_m$  values for  $NADP^{+}$  of *BIIIDH* (19.45  $\mu M$  with  $Mg^{2+}$ ) was similar to those of *L. interrogans* IDH (21.1  $\mu M$ ) [27] and *E. coli* IDH (17  $\mu M$ ) [32], but higher than that of *Rattus norvegicus* cytosolic IDH (11.5  $\mu M$ ) [33] and much lower than those of *Yarrowia lipolytica* IDH (59  $\mu M$ ) [34] and *Helicobacter pylori* IDH (176  $\mu M$ ) [35]. The  $k_{cat}/K_m$  values for  $NADP^{+}$  of *BIIIDH* (1.87  $s^{-1} \cdot \mu M^{-1}$  with  $Mg^{2+}$ ) was higher than that of *H. pylori* IDH (0.704  $s^{-1} \cdot \mu M^{-1}$ ) [35], a member of Type I IDHs subfamily. When compared with other monomeric  $NADP$ -IDHs, in the presence of  $NADP^{+}$ , the coenzyme affinity ( $1/K_m$ ) and the catalytic efficiency (1.87  $s^{-1} \cdot \mu M^{-1}$  with  $Mg^{2+}$  and 0.83  $s^{-1} \cdot \mu M^{-1}$  with  $Mn^{2+}$ ) of *BIIIDH* were quite a bit lower than those of monomeric IDHs, such as *C. glutamicum* IDH (21.75  $s^{-1} \cdot \mu M^{-1}$ ) [28] and *Colwellia maris* IDH (8.9  $s^{-1} \cdot \mu M^{-1}$ ) [36].

#### 2.4. Switch of Coenzyme Specificity

Amino acid sequence alignment, homology modeling and structural analysis of Type II  $NADP$ -IDHs revealed that several amino acid residues in *BIIIDH* may interact with 2'-phosphate moiety of  $NADP^{+}$  directly or indirectly, including Arg314, His315, Thr327, Asp253, Ser257 and Lys260 (Figure 3). To switch coenzyme specificity of *BIIIDH*, these residues were selected as targets for site-directed mutagenesis. Here, only three mutants, single mutant R314D, triple mutant R314D/H315I/T327A and sextuple mutant D253A/S257K/K260Q/R314D/H315I/T327A, displayed detectable activity. Furthermore, circular dichroism (CD) spectra of mutants were very similar to that of wild type (Figure S2), indicating that these six mutations did not cause the conformational alterations of *BIIIDH*.

Kinetic analysis demonstrated that single mutant R314D resulted in an approximate 57-fold increase, from 19.45 to 1102  $\mu\text{M}$ , in  $K_m$  for  $\text{NADP}^+$ , with no significant change in  $K_m$  for  $\text{NAD}^+$  (Table 2). Furthermore, R314D showed a dramatic decrease (984-fold) in  $k_{\text{cat}}/K_m$  toward  $\text{NADP}^+$  coupled with a 16.5-fold decrease in  $k_{\text{cat}}/K_m$  toward  $\text{NAD}^+$ . Thus, the single mutant R314D is still a dual-specificity enzyme with an approximate 9.5-fold preference for  $\text{NADP}^+$  over  $\text{NAD}^+$ , although the wild-type *BIIIDH* exhibited 567-fold preference for  $\text{NADP}^+$ . When another two amino acids (His315 and Thr327) were substituted with Ile315 and Ala327, the triple mutant showed no detectable activity for  $\text{NADP}^+$  but only for  $\text{NAD}^+$ -linked reaction. However, the catalytic efficiency of R314D/H315I/T327A was very poor as compared to wild type (Table 2).

**Table 2.** The kinetic parameters of wild-type *BIIIDH* and mutants.

| Residues at <sup>1</sup> |     |     |     |     |     | NADP <sup>+</sup>       |                                      |   | NAD <sup>+</sup>        |                                      |   | Specificity (A/B) | Specificity (B/A) |
|--------------------------|-----|-----|-----|-----|-----|-------------------------|--------------------------------------|---|-------------------------|--------------------------------------|---|-------------------|-------------------|
| 253                      | 257 | 260 | 314 | 315 | 327 | $K_m$ ( $\mu\text{M}$ ) | $k_{\text{cat}}$ ( $\text{s}^{-1}$ ) | $\frac{k_{\text{cat}}/K_m}{(\text{s}^{-1} \cdot \text{mM}^{-1})}$<br>(A) <sup>2</sup> | $K_m$ ( $\mu\text{M}$ ) | $k_{\text{cat}}$ ( $\text{s}^{-1}$ ) | $\frac{k_{\text{cat}}/K_m}{(\text{s}^{-1} \cdot \text{mM}^{-1})}$<br>(B) <sup>2</sup> |                   |                   |
| D                        | S   | K   | R   | H   | T   | 19.45 ± 2.6             | 36.38 ± 2.1                          | 1870 ± 180  | 3584 ± 238.0            | 11.7 ± 5.2                           | 3.3 ± 0.9   | 567               | 0.0017            |
| (wild-type)              |     |     |     |     |     |                         |                                      |   |                         |                                      |   |                   |                   |
| *                        | *   | *   | D   | *   | *   | 1102 ± 92.6             | 2.15 ± 1.3                           | 1.9 ± 0.7   | 3702 ± 117.1            | 0.88 ± 0.7                           | 0.2 ± 0.1   | 9.5               | 0.105             |
| *                        | *   | *   | D   | I   | *   | -                       | -                                    | -   | -                       | -                                    | -   | -                 | -                 |
| *                        | *   | *   | D   | M   | *   | -                       | -                                    | -   | -                       | -                                    | -   | -                 | -                 |
| *                        | *   | *   | D   | M   | L   | -                       | -                                    | -   | -                       | -                                    | -   | -                 | -                 |
| *                        | *   | *   | D   | I   | A   | -                       | -                                    | -   | 4407 ± 196.7            | 0.41 ± 0.1                           | 0.1 ± 0.01  | -                 | -                 |
| A                        | K   | Q   | D   | I   | A   | 324.1 ± 27.9            | 0.307 ± 0.1                          | 0.95 ± 0.05   | 130 ± 20.9              | 0.518 ± 0.03                         | 4.0 ± 0.5   | 0.2375            | 4.21              |

"-" no apparently detectable activity. The values indicate the means of at least three independent measurements.

<sup>1</sup> D, Aspartic acid; S, Serine; K, Lysine; R, Arginine; H, Histidine; T, Threonine; I, Isoleucine; M, Methionine; L, Leucine; A, Alanine; Q, Glutamine; \*, denote the site without mutation; <sup>2</sup> A,  $k_{\text{cat}}/K_m^{\text{NADP}^+}$ ; B,  $k_{\text{cat}}/K_m^{\text{NAD}^+}$ .

Mutations at six sites caused a 17-fold increase in  $K_m$  for  $\text{NADP}^+$  and a 28-fold decrease in  $K_m$  for  $\text{NAD}^+$  (Figure S1C,D). Furthermore, the catalytic efficiency of sextuple mutant was increased 1.2-fold for  $\text{NAD}^+$  while it retained only about 0.05% catalytic efficiency for  $\text{NADP}^+$ . As a result, the sextuple mutant showed an approximately four-fold preference for  $\text{NAD}^+$  over  $\text{NADP}^+$  [ $(k_{\text{cat}}/K_m)^{\text{NAD}^+}/(k_{\text{cat}}/K_m)^{\text{NADP}^+}$ ], which clearly indicated that the coenzyme specificity of *BIIIDH* was completely converted from  $\text{NADP}^+$  to  $\text{NAD}^+$  by a factor of 2387 via six-residue replacement.

### 3. Discussion

#### 3.1. Coenzyme Specificity Determinants of *BIIIDH*

IDH specificity is governed by residue interactions at three layers [37]. The "First Layer" residues directly contact with the unique 2'-hydroxyl and 2'-phosphate groups of  $\text{NAD(P)}^+$ ; The "Second Layer" residues are more distant amino acids, which can modulate the effects of the first group but not in contact with the unique cofactor moieties; The "Third Layer" residues are far from the cofactor binding site and form long-range interactions, which might promote the formation of a low-energy conformation.

Based on sequence alignment and available structural information, Arg314 and His315 in *BIIIDH* are considered to be the "First Layer" residues, two putative coenzyme specificity determinants, by directly interacting with 2'-phosphate group of  $\text{NADP}^+$ . As expected, the single mutant R314D decreased the affinity for  $\text{NADP}^+$  by approximately 57-fold due to the removal of a salt bridge between Arg314 and 2'-phosphate group of  $\text{NADP}^+$  together with the removal of the electrostatic repulsion between negatively charged Asp and 2'-phosphate group of  $\text{NADP}^+$ . When adjacent His315 was simultaneously mutated to Met or Ile, the resulting double mutant R314D/H315I and R314D/H315M lost activity completely. The loss in  $\text{NADP}^+$ -dependent activity might result from the removal of favorable interactions between Arg314 or His315 and the 2'-phosphate group.

To achieve the  $\text{NAD}^+$ -dependent activity, a third mutation (Thr327Ala) was introduced into the double mutant, creating R314D/H315I/T327A. Here, the residue Thr327 in *BIIIDH* is equivalent to Val351 in *EcIDH* and therefore considered to be the "Second Layer" residue. The crystal structure of

an *Ec*IDH mutant has revealed several essential indirect effects of Val351Ala on specificity alteration, such as to avoid obstructing adenine ring shift and to accommodate the favorable repacking in the adenosine-binding pocket [37]. The similar result has also been reported for *Haloferax volcanii* IDH that the replacement of Val by Ala was crucial for its engineered enzyme to obtain the activity with NAD<sup>+</sup> as a coenzyme [38]. As a result, the triple mutant R314D/H315I/T327A restored partial activity for NAD<sup>+</sup> (Table 3).

**Table 3.** Comparison of kinetic parameters between sextuple mutant and other IDHs.

| Enzymes & Subfamilies  | NAD <sup>+</sup>    |                                     |   | NADP <sup>+</sup>   |                                     |   | Specificity (A/B)      | References |
|--|---------------------|-------------------------------------|---|---------------------|-------------------------------------|---|------------------------|------------|
|  | K <sub>m</sub> (μM) | k <sub>cat</sub> (s <sup>-1</sup> ) | $\frac{k_{cat}}{K_m}$ (s <sup>-1</sup> ·μM <sup>-1</sup> ) (A) <sup>c</sup> | K <sub>m</sub> (μM) | k <sub>cat</sub> (s <sup>-1</sup> ) | $\frac{k_{cat}}{K_m}$ (s <sup>-1</sup> ·μM <sup>-1</sup> ) (B) <sup>c</sup> |                        |            |
| Type I NAD-IDH   |                     |                                     |   |                     |                                     |   |                        |            |
| <i>S. suis</i> NAD-IDH (Mg <sup>2+</sup> ) <sup>a</sup>                  | 233                 | 41                                  | 0.176   | 9527                | 14                                  | 0.0015  | 117                    | [39]       |
| <i>Z. mobilis</i> NAD-IDH (Mg <sup>2+</sup> )                            | 312                 | 88                                  | 0.282   | 8200                | 14                                  | 0.0017  | 165                    | [31]       |
| Engineered <i>E. coli</i> NAD-IDH (Mg <sup>2+</sup> ) <sup>b</sup>       | 99                  | 16.2                                | 0.164   | 5800                | 4.7                                 | 0.00081   | 202                    | [37]       |
| Type II IDH  |                     |                                     |   |                     |                                     |   |                        |            |
| <i>C. litoralis</i> NAD-IDH (Mg <sup>2+</sup> )                          | 262.6               | 36.7                                | 0.140   | -                   | -                                   | -   | -                      | [30]       |
| <i>Micromonas</i> sp. NAD-IDH (Mg <sup>2+</sup> )                        | 126                 | 22.5                                | 0.179   | 1827                | 1.4                                 | 0.0008  | 224                    | [12]       |
| <i>O. lucimarinus</i> NAD-IDH (Mg <sup>2+</sup> )                        | 136.6               | 60.6                                | 0.444   | 2211                | 10.0                                | 0.0045  | 99                     | [12]       |
| <i>O. tauri</i> NAD-IDH (Mg <sup>2+</sup> )                              | 226                 | 59                                  | 0.261   | 3354                | 17                                  | 0.0051  | 51                     | [13]       |
| <i>B. longum</i> NADP-IDH (Mg <sup>2+</sup> )                            | 3584                | 11.70                               | 0.003   | 19.45               | 36.4                                | 1.87  | 0.0016                 | This study |
| Engineered <i>B. longum</i> NAD-IDH (Mg <sup>2+</sup> ) <sup>b</sup>     | 130                 | 0.518                               | 0.004   | 324.1               | 0.307                               | 0.00095   | 4.21                   | This study |
| <i>Y. lipolytica</i> NADP-IDH (Mg <sup>2+</sup> )                        | -                   | -                                   | -   | 59                  | 72                                  | 1.22  | -                      | [34]       |
| Engineered <i>Y. lipolytica</i> NAD-IDH (Mg <sup>2+</sup> ) <sup>b</sup> | 47,000              | 0.38                                | 8.1 × 10 <sup>-6</sup>  | 2410                | 4.24                                | 1750  | 4.6 × 10 <sup>-9</sup> | [34]       |
| Monomeric NAD-IDH  |                     |                                     |   |                     |                                     |   |                        |            |
| <i>Campylobacter</i> sp. NAD-IDH (Mg <sup>2+</sup> )                     | 28.9                | 7.0                                 | 0.242   | 513.2               | 1.9                                 | 0.004   | 61                     | [12]       |
| <i>C. curvus</i> NAD-IDH (Mg <sup>2+</sup> ) <sup>a</sup>                | 74.2                | 10.8                                | 0.146   | 475.9               | 2.0                                 | 0.004   | 37                     | [12]       |

<sup>a</sup> *S. suis*, *Streptococcus suis*; *C. curvus*, *Campylobacter curvus*; “-” not detectable; <sup>b</sup> Engineered *E. coli* NAD-IDH: K344D/Y345I/V351A/Y391K/R395S/C332Y/C201M; Engineered *B. longum* NAD-IDH: D253A/S257K/K260Q/R314D/H315I/T327A; Engineered *Y. lipolytica* NAD-IDH: R322D; <sup>c</sup> A,  $k_{cat}/K_m^{NAD^+}$ ; B,  $k_{cat}/K_m^{NADP^+}$ .

In order to improve the affinity and catalytic activity of R314D/H315I/T327A, a putative residue Asp253 forming hydrogen bond with Arg314 and two putative residues (Ser257 and Lys260) forming extra hydrogen bonds with 2'-phosphate group of NADP<sup>+</sup> were engineered to the corresponding residues in NAD<sup>+</sup>-dependent *O*iIDH (Ala279, Lys283 and Gln286), generating D253A/S257K/K260Q/R314D/H315I/T327A. Compared with the triple mutant (R314D/H315I/T327A), this sextuple mutant showed approximately a 34-fold increase in affinity and a 1.3-fold increase in catalytic activity, resulting in a 40-fold increase in catalytic efficiency for NAD<sup>+</sup>. With respect to the wild-type enzyme, the sextuple mutant displayed a 27.6-fold increase in affinity and a 1.2-fold increase in catalytic efficiency for NAD<sup>+</sup>. As a consequence, the sextuple mutant showed an approximately four-fold preference for NAD<sup>+</sup> over NADP<sup>+</sup> [ $(k_{cat}/K_m)^{NAD^+}/(k_{cat}/K_m)^{NADP^+}$ ]. Therefore, the coenzyme specificity of *B*iIDH was converted from a 567-fold preference for NADP<sup>+</sup> to a four-fold preference for NAD<sup>+</sup> through rational engineering of the major determinants for coenzyme specificity.

### 3.2. Evolutionary Implications for NADP<sup>+</sup> Use by Prokaryotic Type II IDHs

Phylogenetic analysis and competition experiments have revealed that NADP<sup>+</sup> use by bacterial IDHs of Type I subfamily evolved from NAD<sup>+</sup> use about 3.5 billion years ago, and the cause of selection is the NADPH demand for bacterial adaptation to anabolic niches such as acetate [17]. For IDHs of Type I subfamily, their coenzyme specificity can be completely converted from NADP<sup>+</sup> to NAD<sup>+</sup> such as NADP-IDHs from *E. coli* and *H. volcanii* [32,38], or from NAD<sup>+</sup> to NADP<sup>+</sup> such as NAD-IDH from *Pyrococcus furiosus* [40].

The evolutionary origin of Type II subfamily is still obscure because all its members are NADP-dependent IDHs. As more and more genomic sequences have become available, some novel NAD-dependent IDHs are clustered into Type II subfamily after reconstructing the phylogenetic tree of IDHs. We deduce that the ancestor of Type II subfamily is also a NAD-dependent enzyme, the same as that of Type I subfamily. Several NAD-dependent IDHs have converted their coenzyme specificities

from NAD<sup>+</sup> to NADP<sup>+</sup> by strategic amino acid replacements, such as NAD-IDHs from *Micromonas* sp. [12], *O. tauri* [13] and *C. littoralis* [30].

The information about successful inversion of coenzyme specificity in NADP-IDHs of Type II subfamily is very limited. In a previous report, only a single mutant of *Yarrowia lipolytica* NADP-IDH (*YIIDH*, a Type II member), R322D, displayed poor activity for NAD<sup>+</sup> [34]. In this work, the coenzyme specificity of *BIIIDH* mutant was converted from NADP<sup>+</sup> to NAD<sup>+</sup> by a factor of 2387, which is the first case for complete alteration of the coenzyme specificity of Type II NADP-IDHs. However, due to the absence of a putative gene encoding isocitrate lyase in *B. longum* genome, it is unclear whether the coenzyme specificity change of *BIIIDH* was also caused by the increased demand of NADPH under carbon starvation.

## 4. Experimental Section

### 4.1. Sequence Analysis

The X-ray structure of human cytosolic IDH (*HcIDH*) was downloaded from the Protein Data Bank database (available online: <http://www.rcsb.org/pdb/>). SWISS-MODEL server (available online: <http://swissmodel.expasy.org/>) was employed to create the homology model of *BIIIDH* using *HcIDH* structure (PDB code: 1T0L) as a template. Multiple protein sequence alignment was performed using ClustalW program and ESPript 3.0 web tool (available online: <http://esprict.ibcp.fr/ESPript/cgi-bin/ESPript.cgi>). For phylogenetic analysis, 26 protein sequences (including *BIIIDH*) were aligned with ClustalW program. A Neighbor-Joining tree with 500 bootstrap was created via MEGA 6.06 program [41]. Protein structural figures were conducted using PyMOL [42] and UCSF Chimera [43].

### 4.2. Bacterial Strains and Reagents

The *E. coli* strains, DH5 $\alpha$  and Rosetta (DE3), and plasmid pET-28b(+) were stored at low temperature in our laboratory. PrimeSTAR<sup>TM</sup> HS DNA polymerase was purchased from TaKaRa Biotechnology Co., Ltd. (Dalian, China). Restriction endonucleases, T4 DNA ligase and protein molecular weight standards were obtained from Thermo Scientific (Shanghai, China).

### 4.3. Recombinant Plasmid Construction

Genomic DNA of *B. longum* subsp. *infantis* ATCC 15697 was bought from Leibniz Institute DSMZ-German Collection of Microorganisms and Cell Cultures (Braunschweig, Germany). According to the genomic sequence of *B. longum* (NCBI Reference Sequence: NC\_011593.1), one pair of primers (Table S2) were designed to amplify the complete *icd* gene. Initial denaturing step of polymerase chain reaction (PCR) was 3 min at 95 °C, followed by 35 cycles of 95 °C for 30 s, 65 °C for 30 s, and 72 °C for 1 min and 30 s. After Nde I and Not I digestion, the PCR product was cloned into the expression vector pET-28b(+) which has a 6 $\times$ His tag coding sequence upstream of the multiple cloning site. The *icd* gene in the recombinant plasmid pET-*BIIIDH* was sequenced (GenScript, Nanjing, China).

### 4.4. Site-Directed Mutagenesis

In order to identify the determinants and convert the coenzyme specificity of *BIIIDH*, six mutants were created by site-directed mutagenesis and overlap extension PCR technique [44]. The oligonucleotides for constructing the mutants were reported in Table S2. The mutated genes were constructed by sequential PCR steps. In the first step, two fragments containing the desired mutation were amplified with the following primers: *BIIIDH*-S and one of the antisense primers including the point mutation; one of the sense primers including the point mutation and *BIIIDH*-As. Then, the two overlapping fragments were purified and used as templates to amplify the full-length fragment using *BIIIDH*-S and *BIIIDH*-As. The final PCR products were digested by Nde I and Not I and ligated

into the expression vector pET-28b(+). DNA sequencing was performed in both directions to verify all sequences of the mutated genes (GenScript, Nanjing, China).

#### 4.5. Overexpression and Purification

The recombinant expression plasmids were transformed into *E. coli* Rosetta (DE3) strains, and grown overnight at 37 °C in Luria-Bertani (LB) medium supplemented with kanamycin and chloramphenicol to a final concentration of 30 µg/mL. The cultures were inoculated into 100 mL fresh LB media with the same antibiotics. When the optical density at 600 nm (OD<sub>600</sub>) of culture reached 0.4, the isopropyl-1-thio-β-D-galactopyranoside (IPTG) was added to a final concentration of 0.5 mM, followed by continuous growth at 20 °C for 20 h. The cells were collected by centrifugation at 5000 × *g* for 5 min at 4 °C, and sonicated in lysis buffer (50 mM NaH<sub>2</sub>PO<sub>4</sub>, 300 mM NaCl, pH 7.8). The debris was removed by centrifugation at 12,000 × *g* for 20 min at 4 °C. Finally, the recombinant proteins fused with 6×His-tag were purified with BD TALON metal affinity resin according to the manufacturer's instructions (Clontech, Palo Alto, CA, USA).

#### 4.6. SDS-PAGE and Western Blotting

The purity and molecular weight of *BLIDH* were determined by 12% sodium dodecyl sulfate polyacrylamide gel electrophoresis (SDS-PAGE). For the Western blotting analysis, the recombinant enzymes were separated and transferred electrophoretically onto a nitrocellulose membrane. Then, the membrane was blocked for 1 h at room temperature in two solutions, TBS-T buffer (0.2% Tween-20, 150 mM NaCl and 50 mM Tris-HCl at pH 7.5) and 5% skim milk. Next, the membrane was immunoblotted with each antibody for 1 h, anti-6×His-tag polyclonal antibody (cat#2365, Cell Signaling Technology, Danvers, MA, USA, 1:1000) followed by anti-rabbit IgG secondary antibody (cat#S3731, Promega, Madison, WI, USA, 1:2500). After that, the membrane was washed with TBS-T buffer for 10 min for three times. Finally, the chemiluminescence signal was observed by exposing the blot to X-ray film for an appropriate time period in a dark room.

#### 4.7. Gel Filtration Chromatography

Molecular mass and oligomeric states of the recombinant *BLIDH* were measured by gel filtration chromatography on a 10/300 Superdex 200 column (Amersham Biosciences, Freiburg, Germany) with equilibration buffer (50 mM NaH<sub>2</sub>PO<sub>4</sub> and 150 mM NaCl at pH 7.2). The following standards were employed: Ovalbumin (44,000 Da), Conalbumin (75,000 Da), Aldolase (158,000 Da), Ferritin (440,000 Da) and Thyroglobulin (669,000 Da).

#### 4.8. Circular Dichroism Spectroscopy

Circular dichroism (CD) spectra of the recombinant enzymes were measured with a Jasco model J-810 spectropolarimeter. Each sample were prepared in 75 mM Na<sub>2</sub>SO<sub>4</sub> and 20 mM NaH<sub>2</sub>PO<sub>4</sub> at pH 7.5 and then diluted to a final concentration of 0.2 mg/mL. The ellipticity ( $\theta$ ) was generated by averaging 3 scans of the protein solution between 195 and 260 nm at 0.5-nm increments. The mean molar ellipticity,  $[\theta]$  (deg·cm<sup>2</sup>·dmole<sup>-1</sup>), was calculated from  $[\theta] = \theta/10nCl$ , where the relationship has been described previously [45]. The  $\theta$  is the measurement, *n* is the number of residues per subunit of protein (411 amino acids for *BLIDH*), *C* is the molar concentration of the samples, and *l* is the cell path length (0.1 cm).

#### 4.9. Enzyme Assays and Kinetic Characterization

The enzyme assay was described by Cvitkovitch *et al.* [46]. The activity assays were carried out at 25 °C in 1 mL reaction mixture containing 35 mM Tris-HCl at pH 8.0, 2 mM MgCl<sub>2</sub> or MnCl<sub>2</sub>, 1 mM D,L-isocitric acid, and 0.5 mM NADP<sup>+</sup> or 5 mM NAD<sup>+</sup>. The NAD(P)H production was monitored at 340 nm ( $\epsilon_{340} = 6.22 \text{ mM}^{-1} \cdot \text{cm}^{-1}$ ) using Cary300 UV-Vis spectrophotometer (Varian, Palo Alto,

CA, USA). One unit of enzyme activity refers to 1  $\mu\text{M}$  of NAD(P)H formed per minute. The enzyme concentration was detected by using Quick Start Bradford Protein Assay kit (Bio-Rad, Hercules, CA, USA).

To measure the  $K_m$  values of the recombinant enzymes for NAD(P)<sup>+</sup>, the concentration of isocitrate was fixed at 1.0 mM with varying coenzyme concentrations. Apparent  $K_m$  values for NAD(P)<sup>+</sup> were calculated by nonlinear regression with GraphPad Prism 5.0 software (Prism, San Diego, CA, USA) and Origin 8.0 (OriginLab, Northampton, MA, USA). All kinetic parameters were measured in at least three independent experiments.

The effects of temperature, pH and metal ions on *B*IIDH activity were measured using the standard assay method. The optimum pH was determined in the range of 6.0–9.0, and the optimal temperature was measured in the range of 35–60 °C. The half-life of *B*IIDH was tested after incubation of enzyme aliquots at 25–55 °C for 20 min. The effects of metal ions on *B*IIDH activity were also detected, including 2 mM monovalent metal cations (K<sup>+</sup>, Li<sup>+</sup>, Na<sup>+</sup>, and Rb<sup>+</sup>) and divalent metal cations (Mg<sup>2+</sup>, Mn<sup>2+</sup>, Co<sup>2+</sup>, Ca<sup>2+</sup>, Cu<sup>2+</sup>, Zn<sup>2+</sup>, and Ni<sup>2+</sup>).

**Supplementary Materials:** Supplementary materials can be found at <http://www.mdpi.com/1422-0067/17/3/296/s1>.

**Acknowledgments:** This research was supported by the National Natural Science Foundation of China (31570010, 31400003), the Natural Science Foundation of Anhui Province of China (1308085QC67), and the Provincial Project of Natural Science Research for Colleges and Universities of Anhui Province of China (KJ2013A128), Innovation Team of Scientific Research Platform in Anhui Universities and Key Laboratory of the Biotic Environment and Ecological Safety in Anhui Province.

**Author Contributions:** Peng Wang and Guo-Ping Zhu conceived and designed the experiments; Shi-Ping Huang and Hong-Mei Cheng performed the experiments; Shi-Ping Huang, Hong-Mei Cheng and Guo-Ping Zhu analyzed the data; Shi-Ping Huang and Guo-Ping Zhu wrote the paper.

**Conflicts of Interest:** The authors declare no conflict of interest.

## Abbreviations

|                   |   |
|-------------------|---|
| PCR               | polymerase chain reaction                                   |
| LB                | Luria-Bertani   |
| IPTG              | isopropyl-1-thio- $\beta$ -D-galactopyranoside              |
| SDS-PAGE          | sodium dodecyl sulfate polyacrylamide gel electrophoresis   |
| CD                | circular dichroism  |
| SEC               | size exclusion chromatography                               |
| IDH               | isocitrate dehydrogenase                                    |
| NADP <sup>+</sup> | nicotinamide adenine dinucleotide phosphate                 |
| NAD <sup>+</sup>  | nicotinamide adenine dinucleotide                           |
| NADP-IDH          | NADP <sup>+</sup> -dependent isocitrate dehydrogenase       |
| NAD-IDH           | NAD <sup>+</sup> -dependent isocitrate dehydrogenase        |
| <i>B</i> IIDH     | isocitrate dehydrogenase from <i>Bifidobacterium longum</i> |
| <i>E</i> cIDH     | NADP-IDH from <i>Escherichia coli</i>                       |
| <i>H</i> cIDH     | human cytosolic NADP-IDH                                    |
| <i>A</i> tIDH     | NAD-IDH from <i>Acidithiobacillus thiooxidans</i>           |
| <i>O</i> tIDH     | NAD-IDH from <i>Ostreococcus tauri</i>                      |
| $K_m$             | Michaelis constant  |
| $k_{\text{cat}}$  | catalytic rate constant                                     |

## References

1. Sivaraman, J.; Li, Y.; Banks, J.; Cane, D.E.; Matte, A.; Cygler, M. Crystal structure of *Escherichia coli* PdxA, an enzyme involved in the pyridoxal phosphate biosynthesis pathway. *J. Biol. Chem.* **2003**, *278*, 43682–43690. [[CrossRef](#)] [[PubMed](#)]
2. Miyazaki, J.; Kobashi, N.; Nishiyama, M.; Yamane, H. Characterization of homoisocitrate dehydrogenase involved in lysine biosynthesis of an extremely thermophilic bacterium, *Thermus thermophilus* HB27, and evolutionary implication of  $\beta$ -decarboxylating dehydrogenase. *J. Biol. Chem.* **2003**, *278*, 1864–1871. [[CrossRef](#)] [[PubMed](#)]
3. Tipton, P.A.; Beecher, B.S. Tartrate dehydrogenase, a new member of the family of metal-dependent decarboxylating R-hydroxyacid dehydrogenases. *Arch. Biochem. Biophys.* **1994**, *313*, 15–21. [[CrossRef](#)] [[PubMed](#)]
4. Dean, A.M.; Koshland, D.E., Jr. Kinetic mechanism of *Escherichia coli* isocitrate dehydrogenase. *Biochemistry* **1993**, *32*, 9302–9309. [[CrossRef](#)] [[PubMed](#)]
5. Fernie, A.R.; Carrari, F.; Sweetlove, L.J. Respiratory metabolism: Glycolysis, the TCA cycle and mitochondrial electron transport. *Curr. Opin. Plant Biol.* **2004**, *7*, 254–261. [[CrossRef](#)] [[PubMed](#)]
6. Spaans, S.K.; Weusthuis, R.A.; van der Oost, J.; Kengen, S.W. NADPH-generating systems in bacteria and archaea. *Front. Microbiol.* **2015**, *6*. [[CrossRef](#)] [[PubMed](#)]
7. Lee, S.M.; Koh, H.J.; Park, D.C.; Song, B.J.; Huh, T.L.; Park, J.W. Cytosolic NADP<sup>+</sup>-dependent isocitrate dehydrogenase status modulates oxidative damage to cells. *Free Radic. Biol. Med.* **2002**, *32*, 1185–1196. [[CrossRef](#)]
8. Jo, S.H.; Son, M.K.; Koh, H.J.; Lee, S.M.; Song, I.H.; Kim, Y.O.; Lee, Y.S.; Jeong, K.S.; Kim, W.B.; Park, J.W.; *et al.* Control of mitochondrial redox balance and cellular defense against oxidative damage by mitochondrial NADP<sup>+</sup>-dependent isocitrate dehydrogenase. *J. Biol. Chem.* **2001**, *276*, 16168–16176. [[CrossRef](#)] [[PubMed](#)]
9. Cohen, A.L.; Holmen, S.L.; Colman, H. IDH1 and IDH2 mutations in gliomas. *Curr. Neurol. Neurosci. Rep.* **2013**, *13*, 345. [[CrossRef](#)] [[PubMed](#)]
10. Chen, C.; Liu, Y.; Lu, C.; Cross, J.R.; Morris, J.P.; Shroff, A.S.; Ward, P.S.; Bradner, J.E.; Thompson, C.; Lowe, S.W. Cancer-associated IDH2 mutants drive an acute myeloid leukemia that is susceptible to Brd4 inhibition. *Genes Dev.* **2013**, *27*, 1974–1985. [[CrossRef](#)] [[PubMed](#)]
11. Dang, L.; White, D.W.; Gross, S.; Bennett, B.D.; Bittinger, M.A.; Driggers, E.M.; Fantin, V.R.; Jang, H.G.; Jin, S.; Keenan, M.C.; *et al.* Cancer-associated IDH1 mutations produce 2-hydroxyglutarate. *Nature* **2009**, *462*, 739–744. [[CrossRef](#)] [[PubMed](#)]
12. Wang, P.; Lv, C.; Zhu, G. Novel type II and monomeric NAD<sup>+</sup> specific isocitrate dehydrogenases: Phylogenetic affinity, enzymatic characterization, and evolutionary implication. *Sci. Rep.* **2015**, *5*. [[CrossRef](#)] [[PubMed](#)]
13. Tang, W.G.; Song, P.; Cao, Z.Y.; Wang, P.; Zhu, G.P. A unique homodimeric NAD<sup>+</sup>-linked isocitrate dehydrogenase from the smallest autotrophic eukaryote *Ostreococcus tauri*. *FASEB J.* **2015**, *29*, 2462–2472. [[CrossRef](#)]
14. Peng, Y.; Zhong, C.; Huang, W.; Ding, J. Structural studies of *Saccharomyces cerevesiae* mitochondrial NADP-dependent isocitrate dehydrogenase in different enzymatic states reveal substantial conformational changes during the catalytic reaction. *Protein Sci.* **2008**, *17*, 1542–1554. [[CrossRef](#)] [[PubMed](#)]
15. Xu, X.; Zhao, J.; Xu, Z.; Peng, B.; Huang, Q.; Arnold, E.; Ding, J. Structures of human cytosolic NADP-dependent isocitrate dehydrogenase reveal a novel self-regulatory mechanism of activity. *J. Biol. Chem.* **2004**, *279*, 33946–33957. [[CrossRef](#)] [[PubMed](#)]
16. Ceccarelli, C.; Grodsky, N.B.; Ariyaratne, N.; Colman, R.F.; Bahnson, B.J. Crystal structure of porcine mitochondrial NADP<sup>+</sup>-dependent isocitrate dehydrogenase complexed with Mn<sup>2+</sup> and isocitrate. Insights into the enzyme mechanism. *J. Biol. Chem.* **2002**, *277*, 43454–43462. [[CrossRef](#)] [[PubMed](#)]
17. Zhu, G.; Golding, G.B.; Dean, A.M. The selective cause of an ancient adaptation. *Science* **2005**, *307*, 1279–1282. [[CrossRef](#)] [[PubMed](#)]
18. Srutkova, D.; Spanova, A.; Spano, M.; Drab, V.; Schwarzer, M.; Kozakova, H.; Rittich, B. Efficiency of PCR-based methods in discriminating *Bifidobacterium longum* ssp. *longum* and *Bifidobacterium longum* ssp. *infantis* strains of human origin. *J. Microbiol. Methods* **2011**, *87*, 10–16. [[CrossRef](#)] [[PubMed](#)]

19. Yuan, J.; Zhu, L.; Liu, X.; Li, T.; Zhang, Y.; Ying, T.; Wang, B.; Wang, J.; Dong, H.; Feng, E.; *et al.* A proteome reference map and proteomic analysis of *Bifidobacterium longum* NCC2705. *Mol. Cell. Proteom.* **2006**, *5*, 1105–1118. [[CrossRef](#)] [[PubMed](#)]
20. Schell, M.A.; Karmirantzou, M.; Snel, B.; Vilanova, D.; Berger, B.; Pessi, G.; Zwahlen, M.C.; Desiere, F.; Bork, P.; Delley, M.; *et al.* The genome sequence of *Bifidobacterium longum* reflects its adaptation to the human gastrointestinal tract. *Proc. Natl. Acad. Sci. USA* **2002**, *99*, 14422–14427. [[CrossRef](#)] [[PubMed](#)]
21. Lin, M.Y.; Chang, F.J. Antioxidative effect of intestinal bacteria *Bifidobacterium longum* ATCC 15708 and *Lactobacillus acidophilus* ATCC 4356. *Dig. Dis. Sci.* **2000**, *45*, 1617–1622. [[CrossRef](#)] [[PubMed](#)]
22. Iwabuchi, N.; Xiao, J.Z.; Yaeshima, T.; Iwatsuki, K. Oral administration of *Bifidobacterium longum* ameliorates influenza virus infection in mice. *Biol. Pharm. Bull.* **2011**, *34*, 1352–1355. [[CrossRef](#)] [[PubMed](#)]
23. Xiao, J.Z.; Kondo, S.; Yanagisawa, N.; Miyaji, K.; Enomoto, K.; Sakoda, T.; Iwatsuki, K.; Enomoto, T. Clinical efficacy of probiotic *Bifidobacterium longum* for the treatment of symptoms of Japanese cedar pollen allergy in subjects evaluated in an environmental exposure unit. *Allergol. Int.* **2007**, *56*, 67–75. [[CrossRef](#)] [[PubMed](#)]
24. Sivan, A.; Corrales, L.; Hubert, N.; Williams, J.B.; Aquino-Michaels, K.; Earley, Z.M.; Benyamin, F.W.; Lei, Y.M.; Jabri, B.; Alegre, M.L.; *et al.* Commensal *Bifidobacterium* promotes antitumor immunity and facilitates anti-PD-L1 efficacy. *Science* **2015**, *350*, 1084–1089. [[CrossRef](#)] [[PubMed](#)]
25. Yazawa, K.; Fujimori, M.; Amano, J.; Kano, Y.; Taniguchi, S. *Bifidobacterium longum* as a delivery system for cancer gene therapy: Selective localization and growth in hypoxic tumors. *Cancer Gene Ther.* **2000**, *7*, 269–274. [[CrossRef](#)] [[PubMed](#)]
26. Imada, K.; Tamura, T.; Takenaka, R.; Kobayashi, I.; Namba, K.; Inagaki, K. Structure and quantum chemical analysis of NAD<sup>+</sup>-dependent isocitrate dehydrogenase: Hydride transfer and co-factor specificity. *Proteins* **2008**, *70*, 63–71. [[CrossRef](#)] [[PubMed](#)]
27. Zhao, X.; Wang, P.; Zhu, G.; Wang, B.; Zhu, G. Enzymatic characterization of a type II isocitrate dehydrogenase from pathogenic *Leptospira interrogans* serovar Lai strain 56601. *Appl. Biochem. Biotechnol.* **2014**, *172*, 487–496. [[CrossRef](#)] [[PubMed](#)]
28. Chen, R.; Yang, H. A highly specific monomeric isocitrate dehydrogenase from *Corynebacterium glutamicum*. *Arch. Biochem. Biophys.* **2000**, *383*, 238–245. [[CrossRef](#)] [[PubMed](#)]
29. Kanao, T.; Kawamura, M.; Fukui, T.; Atomi, H.; Imanaka, T. Characterization of isocitrate dehydrogenase from the green sulfur bacterium *Chlorobium limicola*. *Eur. J. Biochem.* **2002**, *269*, 1926–1931. [[CrossRef](#)] [[PubMed](#)]
30. Wu, M.C.; Tian, C.Q.; Cheng, H.M.; Xu, L.; Wang, P.; Zhu, G.P. A novel type II NAD<sup>+</sup>-specific isocitrate dehydrogenase from the marine bacterium *Congregibacter litoralis* KT71. *PLoS ONE* **2015**, *10*, e0125229. [[CrossRef](#)] [[PubMed](#)]
31. Wang, P.; Jin, M.; Zhu, G. Biochemical and molecular characterization of NAD<sup>+</sup>-dependent isocitrate dehydrogenase from the ethanologenic bacterium *Zymomonas mobilis*. *FEMS Microbiol. Lett.* **2012**, *327*, 134–141. [[CrossRef](#)] [[PubMed](#)]
32. Dean, A.M.; Golding, G.B. Protein engineering reveals ancient adaptive replacements in isocitrate dehydrogenase. *Proc. Natl. Acad. Sci. USA* **1997**, *94*, 3104–3109. [[CrossRef](#)] [[PubMed](#)]
33. Jennings, G.T.; Minard, K.I.; McAlister-Henn, L. Expression and mutagenesis of mammalian cytosolic NADP<sup>+</sup>-specific isocitrate dehydrogenase. *Biochemistry* **1997**, *36*, 13743–13747. [[CrossRef](#)] [[PubMed](#)]
34. Li, X.; Wang, P.; Ge, Y.; Wang, W.; Abbas, A.; Zhu, G. NADP<sup>+</sup>-specific isocitrate dehydrogenase from oleaginous yeast *Yarrowia lipolytica* CLIB122: Biochemical characterization and coenzyme sites evaluation. *Appl. Biochem. Biotechnol.* **2013**, *171*, 403–416. [[CrossRef](#)] [[PubMed](#)]
35. Huang, D.; Liu, J.; Shen, G. Cloning, expression, and enzymatic characterization of isocitrate dehydrogenase from *Helicobacter pylori*. *Protein J.* **2009**, *28*, 443–447. [[CrossRef](#)] [[PubMed](#)]
36. Watanabe, S.; Yasutake, Y.; Tanaka, I.; Takada, Y. Elucidation of stability determinants of cold-adapted monomeric isocitrate dehydrogenase from a psychrophilic bacterium, *Colwellia maris*, by construction of chimeric enzymes. *Microbiology* **2005**, *151*, 1083–1094. [[CrossRef](#)] [[PubMed](#)]
37. Hurley, J.H.; Chen, R.; Dean, A.M. Determinants of cofactor specificity in isocitrate dehydrogenase: Structure of an engineered NADP<sup>+</sup>→NAD<sup>+</sup> specificity-reversal mutant. *Biochemistry* **1996**, *35*, 5670–5678. [[CrossRef](#)] [[PubMed](#)]

38. Rodriguez-Arnedo, A.; Camacho, M.; Llorca, F.; Bonete, M.J. Complete reversal of coenzyme specificity of isocitrate dehydrogenase from *Haloferax volcanii*. *Protein J.* **2005**, *24*, 259–266. [[CrossRef](#)] [[PubMed](#)]
39. Wang, P.; Jin, M.; Su, R.; Song, P.; Wang, M.; Zhu, G. Enzymatic characterization of isocitrate dehydrogenase from an emerging zoonotic pathogen *Streptococcus suis*. *Biochimie* **2011**, *93*, 1470–1475. [[CrossRef](#)] [[PubMed](#)]
40. Steen, I.H.; Lien, T.; Madsen, M.S.; Birkeland, N.K. Identification of cofactor discrimination sites in NAD-isocitrate dehydrogenase from *Pyrococcus furiosus*. *Arch. Microbiol.* **2002**, *178*, 297–300. [[CrossRef](#)] [[PubMed](#)]
41. Tamura, K.; Stecher, G.; Peterson, D.; Filipski, A.; Kumar, S. MEGA6: Molecular evolutionary genetics analysis version 6.0. *Mol. Biol. Evol.* **2013**, *30*, 2725–2729. [[CrossRef](#)] [[PubMed](#)]
42. Bramucci, E.; Paiardini, A.; Bossa, F.; Pascarella, S. PyMod: Sequence similarity searches, multiple sequence-structure alignments, and homology modeling within PyMOL. *BMC Bioinform.* **2012**, *13*. [[CrossRef](#)] [[PubMed](#)]
43. Pettersen, E.F.; Goddard, T.D.; Huang, C.C.; Couch, G.S.; Greenblatt, D.M.; Meng, E.C.; Ferrin, T.E. UCSF Chimera—A visualization system for exploratory research and analysis. *J. Comput. Chem.* **2004**, *25*, 1605–1612. [[CrossRef](#)] [[PubMed](#)]
44. Ho, S.N.; Hunt, H.D.; Horton, R.M.; Pullen, J.K.; Pease, L.R. Site-directed mutagenesis by overlap extension using the polymerase chain-reaction. *Gene* **1989**, *77*, 51–59. [[CrossRef](#)]
45. Pace, C.N.; Vajdos, F.; Fee, L.; Grimsley, G.; Gray, T. How to measure and predict the molar absorption coefficient of a protein. *Protein Sci.* **1995**, *4*, 2411–2423. [[CrossRef](#)] [[PubMed](#)]
46. Cvitkovitch, D.G.; Gutierrez, J.A.; Bleiweis, A.S. Role of the citrate pathway in glutamate biosynthesis by *Streptococcus mutans*. *J. Bacteriol.* **1997**, *179*, 650–655. [[PubMed](#)]



© 2016 by the authors; licensee MDPI, Basel, Switzerland. This article is an open access article distributed under the terms and conditions of the Creative Commons by Attribution (CC-BY) license (<http://creativecommons.org/licenses/by/4.0/>).